ChemPubSoc Europe

DOI: 10.1002/cmdc.201500334

CHEMMEDCHEM Full Papers

6-Methyluracil Derivatives as Bifunctional Acetylcholinesterase Inhibitors for the Treatment of Alzheimer's Disease

Vyacheslav E. Semenov,*[a] Irina V. Zueva,[a, b] Marat A. Mukhamedyarov,[c] Sofya V. Lushchekina,[a, d] Alexandra D. Kharlamova,[a] Elena O. Petukhova,[c] Anatoly S. Mikhailov,[a] Sergey N. Podyachev,[a] Lilya F. Saifina,[a] Konstantin A. Petrov,[a, b, e] Oksana A. Minnekhanova,[a] Vladimir V. Zobov,[a, b] Evgeny E. Nikolsky,[a, b, c, e] Patrick Masson,[b] and Vladimir S. Reznik[a]

Novel 6-methyluracil derivatives with ω-(substituted benzylethylamino)alkyl chains at the nitrogen atoms of the pyrimidine ring were designed and synthesized. The numbers of methylene groups in the alkyl chains were varied along with the electron-withdrawing substituents on the benzyl rings. The compounds are mixed-type reversible inhibitors of cholinesterases, and some of them show remarkable selectivity for human acetylcholinesterase (hAChE), with inhibitory potency in the nanomolar range, more than 10000-fold higher than that for human butyrylcholinesterase (hBuChE). Molecular modeling studies indicate that these compounds are bifunctional AChE inhibitors, spanning the enzyme active site gorge and binding to its peripheral anionic site (PAS). In vivo experiments show that the 6-methyluracil derivatives are able to penetrate the blood–brain barrier (BBB), inhibiting brain-tissue AChE. The most potent AChE inhibitor, **3d** (1,3-bis[5-(*o*-nitrobenzylethylamino)pentyl]-6-methyluracil), was found to improve working memory in scopolamine and transgenic APP/PS1 murine models of Alzheimer's disease, and to significantly decrease the number and area of β-amyloid peptide plaques in the brain.

Introduction

Alzheimer's disease (AD) is the primary age-related neurodegenerative disorder. It is characterized by memory loss and progressive cognitive impairment. The brains of AD patients suffer from loss of cholinergic neurons and a decreased number of synapses in specific areas, including the hippocampus, basal forebrain, and cortex areas involved in learning and memory.[1] The pathogenesis of AD is not completely understood, and multiple factors contribute to neuronal cell death to various extents.[2,3]

Most notably, AD is characterized by increased amounts of soluble and insoluble β-amyloid (Aβ), predominantly in the forms of $A\beta_{42}$ in amyloid plaques and $A\beta_{40}$ in amyloid angiopathy. The amyloid hypothesis proposes that AD is caused by an imbalance between Aβ production and clearance, resulting in increased amounts of Aβ in various forms such as monomer, oligomers, insoluble fibrils, and plaques. High levels of Aβ then initiate a cascade of events culminating in neuronal death, manifesting as progressive memory impairment.[4,5]

Decreases in Aβ production and increased clearance of Aβ pathogenic forms are key targets in the development of novel drugs for AD treatment. Unfortunately, only nootropic approaches for the treatment of AD are currently efficient in humans. These approaches focus mainly on the inhibition of brain acetylcholinesterase (AChE) to increase the lifetime of cerebral acetylcholine and slow down patients' cholinergic deficiency. Three AChE inhibitors (donepezil, rivastigmine, and galantamine) have been approved by drug and sanitary agencies for palliative treatment of mild to moderately severe AD. These drugs are able to improve memory and cognitive dysfunctions, but unfortunately, are unable to slow down neurodegeneration.[6,7]

[a] *Dr. V. E. Semenov, I. V. Zueva, Dr. S. V. Lushchekina, Dr. A. D. Kharlamova, Dr. A. S. Mikhailov, Dr. S. N. Podyachev, Dr. L. F. Saifina, Dr. K. A. Petrov, O. A. Minnekhanova, Prof. V. V. Zobov, Prof. E. E. Nikolsky, Prof. V. S. Reznik*
A.E. Arbuzov Institute of Organic & Physical Chemistry
Kazan Scientific Center, Russian Academy of Sciences
Arbuzov str. 8, Kazan 420088 (Russia)
E-mail: sve@iopc.ru

[b] *I. V. Zueva, Dr. K. A. Petrov, Prof. V. V. Zobov, Prof. E. E. Nikolsky, Prof. P. Masson*
Kazan Federal University
Kremlevskaya str. 18, Kazan 420008 (Russia)

[c] *Dr. M. A. Mukhamedyarov, E. O. Petukhova, Prof. E. E. Nikolsky*
Kazan State Medical University
Butlerov str. 49, Kazan 420012 (Russia)

[d] *Dr. S. V. Lushchekina*
N.M. Emanuel Institute of Biochemical Physics
Kosygin str. 4, Moscow 119991 (Russia)

[e] *Dr. K. A. Petrov, Prof. E. E. Nikolsky*
Kazan Institute of Biochemistry & Biophysics, Russian Academy of Sciences
Lobachevsky str. 2/31, Kazan 420111 (Russia)

Supporting information for this article is available on the WWW under http://dx.doi.org/10.1002/cmdc.201500334.

It is important to emphasize that AChE itself, in addition to an imbalance in the Aβ cascade, promotes the formation of Aβ fibrils in vitro and Aβ plaques in the cerebral cortex of transgenic mouse models of AD.[8] This property of AChE results from the interaction between Aβ and the peripheral anionic site (PAS) of the enzyme.[9] In brain, the sister enzyme butyrylcholinesterase (BChE) is found in neurons and glial cells as well as in neuritic plaques and tangles in AD patients.[10] However, it was observed that amyloid only interacts with the PAS of AChE. BChE acts as a negative modifier capable of suppressing AChE-enhanced facilitation of amyloid fibril formation.[11–13] Therefore, only selective AChE inhibitors are promising as disease-modifying compounds with respect to Aβ aggregation.

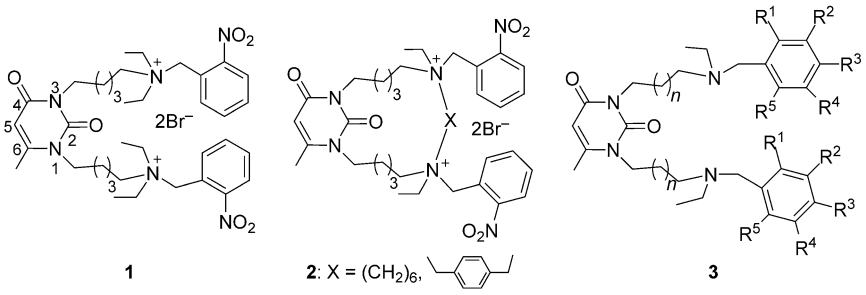

Figure 1. Structures of acyclic and macrocyclic AChE inhibitors containing the 1,3-bis[5-(*o*-nitrobenzylethylammonium)pentyl)-6-methyluracilic moiety (compounds **1** and **2**) and their uncharged counterparts **3**.

We must point out that BChE is present in human plasma (its average concentration is 50 nM), and that clinical studies have shown that inhibition of plasma BChE may potentiate adverse side effects.[14,15] Moreover, the activity of BChE is variable in human populations due to large genetic polymorphism,[16] and due to physiological status. Therefore, doses of BChE inhibitors needed for patients vary between individuals. Thus, nonspecific AChE/BChE inhibitors such as rivastigmine are more difficult to use because they react first in the bloodstream with plasma BChE. Otherwise, the plasma BChE issue does not affect the action of highly selective AChE inhibitors.

The discovery that PAS ligands preclude AChE-induced Aβ aggregation in vitro has led to the development of dual binding site inhibitors of both the catalytic active site (CAS) and PAS. These inhibitors span the active site gorge of the enzyme.[17–19] Dual binding site inhibitors—bifunctional inhibitors—are promising anti-AD drug candidates. Indeed, they can simultaneously improve cognition and slow the rate of Aβ-induced neural degeneration. To assess the possible extent of disease-modifying effects with respect to Aβ aggregation, PAS inhibitors of different structure must be studied on models of AD in vivo, characterized by impairment of the amyloid cascade events. This proposal was recently validated in transgenic animal models of AD. It showed an improvement in cognition and a decrease in brain amyloid plaque levels if transgenic mice were treated with dual binding site AChE inhibitors.[20,21] Unfortunately, the assortment of AChE PAS ligands, as potential drugs, that have been validated in animal models of AD with amyloidosis is still extremely limited.

We previously described a new class of selective mammalian AChE vs. butyrylcholinesterase (BChE) inhibitors with acyclic and macrocyclic structures based on the 1,3-bis[5-(*o*-nitrobenzylethylammonium)pentyl]-6-methyluracil unit.[22,23] In particular, compound **1** and macrocyclic counterparts **2** are shown in Figure 1. Docking studies indicate these onium derivatives of 6-methyluracil bind to the CAS as well as to the PAS; that is, they occupy the whole gorge of AChE from active site to the PAS. These compounds are dual binding site (bifunctional) inhibitors. They were tested in an animal model of myasthenia gravis and may be considered as valuable candidates for the treatment of pathological muscle-weakness syndromes.[23]

It is clear that inhibitors **1** and **2** cannot cross the blood–brain barrier (BBB) due to the quaternary nitrogen atoms in their structure. In continuation of research on new AChE inhibitors among 5(6)-substituted uracil derivatives, we aimed to study the putative advantages of AChE non-charged PAS inhibitors based on 1,3-bis(ω-ethylaminoalkyl)-6-methyluracil derivatives for the treatment of AD (compounds **3**; Figure 1). These compounds, namely 1,3-bis[ω-(substituted benzylethylamino)alkyl]-6-methyluracils, possess both the 1,3-bis[ω-(ethylamino)alkyl]-6-methyluracilic and substituted benzylic moieties. However, unlike onium uracils **1** and **2**, they do not contain quaternary nitrogen atoms. To elucidate structure–activity relationships, the substituted benzylethylamino groups were bridged to the nitrogen atoms of the 6-methyluracil moiety, using various polymethylene chains, in particular tetra-, penta-, and hexamethylene chains (Figure 1). In addition, the electron-withdrawing substituents on the benzyl rings were also varied. Thus, compounds **3** were expected to be able to cross the BBB. Because compounds **1** and **2** are bifunctional inhibitors of AChE, we consider their uncharged counterparts **3** as potent inhibitors for the treatment of AD symptoms. Herein we present results obtained with compounds **3** from: 1) in vitro experiments (kinetic analysis of both human AChE and BChE inhibition, determination of inhibitor selectivity, inhibition of AChE-induced $A\beta_{1-40}$ peptide aggregation); 2) in silico studies (molecular docking of compounds **3** into the active site gorge and to the PAS of human AChE); 3) in vivo experiments (toxicology and pharmacology): determination of LD_{50}, penetration of compounds across the BBB, memory performance studies on mouse models (scopolamine model and early-onset AD transgenic mice), and behavioral tests. The results indicate that certain bifunctional compounds **3** are promising candidates for the palliative treatment of AD.

Results and Discussion

Chemistry

The target compounds **3** were synthesized by starting from substituted benzyl bromide **4** and diamines **5a–c**, the latter of which were obtained from dibromides **6** and ethylamine. This step was described elsewhere.[24,25] Scheme 1 shows the steps leading to bisamines **3**.

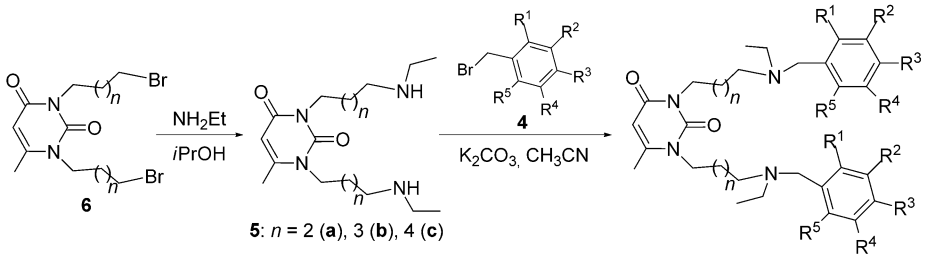

3: *n* = 2: $R^1 = NO_2$, $R^2 = R^3 = R^4 = R^5 = H$ (**a**);
$R^1 = CF_3$, $R^2 = R^3 = R^4 = R^5 = H$ (**b**);
$R^1 = NO_2$, $R^2 = R^3 = R^4 = H$, $R^5 = F$ (**c**);
n = 3: $R^1 = NO_2$, $R^2 = R^3 = R^4 = R^5 = H$ (**d**);
$R^1 = CF_3$, $R^2 = R^3 = R^4 = R^5 = H$ (**e**);
$R^1 = NO_2$, $R^2 = R^3 = R^4 = H$, $R^5 = F$ (**f**);
$R^1 = R^3 = CF_3$, $R^2 = R^4 = R^5 = H$ (**g**);
$R^1 = CF_3$, $R^2 = R^3 = R^4 = H$, $R^5 = F$ (**h**);
$R^1 = R^2 = R^3 = R^4 = R^5 = F$ (**i**);
n = 4: $R^1 = NO_2$, $R^2 = R^3 = R^4 = R^5 = H$ (**j**);
$R^1 = CF_3$, $R^2 = R^3 = R^4 = R^5 = H$ (**k**)

Scheme 1. Synthesis of AChE inhibitors based on 1,3-bis(ω-ethylaminoalkyl)-6-methyluracilic derivatives.

Pharmacology

The inhibitory potency of compounds **3a–k** and reference compound donepezil hydrochloride, against hAChE (recombinant human AChE) and hBChE (from human serum) was measured using the method of Ellman et al.[26] The IC_{50} values of all compounds are in nanomolar range, and their selectivity indexes for AChE over BChE are listed in Table 1, in which compounds are arranged according their structural features. In particular, among compounds **3a**,**d**,**j** and **3b**,**e**,**k**, the number of methylene groups (*n*) varied from 4 to 6 provided that the *o*-nitro- and *o*-trifluoromethyl substituents, respectively, on the phenyl rings remain unchanged. Compounds **3c**,**f** contain tetra- and pentamethylene chains with *o*-nitro and *o*-fluoro substituents on phenyl rings, and the pentamethylene chains of compounds **3g–i** are terminated with *o*-trifluoro-*p*-trifluoromethyl-, *o*-trifluoromethyl-*o*-fluoro-, and pentafluorobenzyl moieties, respectively.

It is clear from the SAR profile of the 1,3-bis[ω-(substituted benzylethylamino)alkyl]-6-methyluracil derivatives that the number of methylene groups in the alkyl spacers and the nature of substituents on benzyl moieties greatly influence the inhibitory potency against AChE and BChE. An increase in the polymethylene N_{uracil}-N-chain length up to five methylene units in compounds **3d** and **3e** markedly increased the strength of AChE inhibition relative to donepezil hydrochloride, whereas an *o*-trifluoromethyl substituent on the benzyl moieties provided remarkable selectivity for AChE vs. BChE, contrary to the *o*-nitro substituent. The following increase in polymethylene chain length up to six methylene groups in compounds **3j** and **3k** diminished inhibitory potency toward AChE. Notably, compounds **3a** and **3b** with 4-(*o*-nitro- and *o*-trifluoromethylbenzylethylamino)tetramethylene chains exhibited selectivity for AChE vs. BChE higher than that of donepezil hydrochloride. The same trend, namely an increase in efficacy of compounds with increased polymethylene chain length, was observed for compounds **3c**,**f** with two substituents, nitro- and fluoro, at the *ortho* positions of the phenyl rings. However, it is clear that the introduction of additive fluoro groups impaired anti-AChE potency relative to compounds **3a**,**d**, with only the *o*-nitro group on phenyl rings. Introduction of additional substituents with fluorine atoms onto the benzyl moieties, in particular two trifluoromethyl groups (compound **3g**), fluoro- and trifluoromethyl groups (compound **3h**), and five fluoro groups (compound **3i**), diminished the inhibitory potency toward AChE,

Table 1. In vitro inhibition of AChE from human erythrocytes and human serum BChE by compounds **3a–k** compared with donepezil hydrochloride.

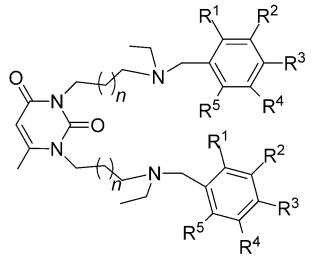

Compd	*n*	$R^{n[c]}$	IC_{50} [nM][a] AChE	IC_{50} [nM][a] BChE	SI[b]
3a	2	$R^1 = NO_2$	47 ± 3	50 000 ± 3000	1100
3d	3	$R^1 = NO_2$	3.5 ± 0.5	35 000 ± 500	10 000
3j	4	$R^1 = NO_2$	83 ± 10	90 000 ± 3000	1100
3b	2	$R^1 = CF_3$	67 ± 8	20 000 ± 1300	300
3e	3	$R^1 = CF_3$	5.6 ± 0.7	200 000 ± 2000	36 000
3k	4	$R^1 = CF_3$	1400 ± 90	200 000 ± 2100	150
3c	2	$R^1 = NO_2$, $R^5 = F$	527 ± 35	50 000 ± 3000	100
3f	3	$R^1 = NO_2$, $R^5 = F$	44 ± 4	20 000 ± 1800	450
3g	3	$R^1 = R^3 = CF_3$	10 700 ± 96	100 000 ± 12 000	9
3h	3	$R^1 = CF_3$, $R^5 = F$	154 ± 8	10 000 ± 900	65
3i	3	$R^1 = R^2 = R^3 = R^4 = R^5 = F$	21 ± 2	810 ± 75	40
donepezil·HCl			48 ± 3.2	7900 ± 600	160

[a] Values are the mean ± SEM of *n* = 3 independent measurements performed in duplicate; acetylthiocholine (ATCh) or butyrylthiocholine (BuTCh) concentration was 1 mM. [b] AChE selectivity index: ($IC_{50\ BChE}$)/($IC_{50\ AChE}$). [c] R^n = H unless otherwise indicated.

thereby decreasing selectivity for AChE vs. BChE, relative to compounds **3b**,**e** with only an *o*-trifluoromethyl group on the phenyl rings. Thus, analysis of the data in Table 1 shows that 5-(*o*-nitro- and *o*-trifluoromethylbenzylethylamino)pentamethylene chains linked to the nitrogen atoms of uracil are optimal for the inhibition of AChE. Compounds **3d**,**e** inhibited AChE in the nanomolar range with remarkable selectivity for AChE vs. BChE.

To investigate the AChE and BChE inhibitory mechanism for this class of compounds, the most active compound **3d** (one of the lowest IC_{50} values for AChE) was selected for kinetic study. For determining inhibition type and inhibition constants (K_i), experiments were performed using three different concentrations of acetylthiocholine (ATCh) as substrate for AChE or butyrylthiocholine (BuTCh) for BChE. Dixon (Figure 2A,C) and

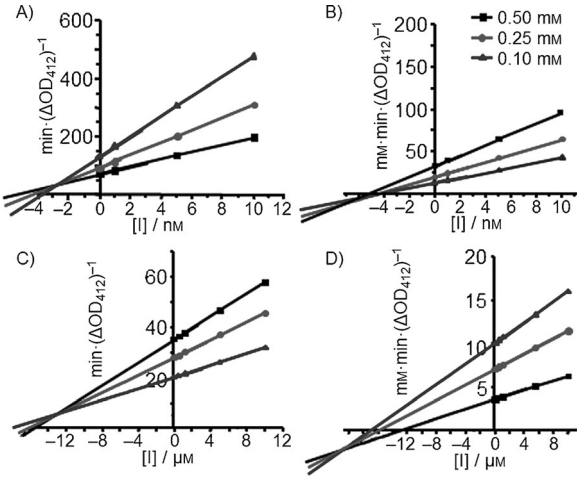

Figure 2. Dixon plots for the inhibition of A) AChE and C) BChE by **3d**; $K_{i,c}$ is the abscissa of the intersecting point. Cornish-Bowden plots for the inhibition of B) AChE and D) BChE by **3d**; $K_{i,nc}$ is the abscissa of the intersecting point. The three different substrate concentrations used (ATCh for AChE, BuTCh for BChE) are indicated at upper right.

Cornish-Bowden plots (Figure 2B,D) showed that the inhibition of AChE and BChE by compound **3d** is of mixed type, with inhibition constants $K_{i,c} = 2.7$ nM (AChE), $K_{i,c} = 13.6$ μM (BChE) for the competitive (c) component, and $K_{i,nc} = 5.71$ nM (AChE), $K_{i,nc} = 22.3$ μM (BChE) for the non-competitive (nc) component.

Molecular modeling

To validate the docking procedure, donepezil was re-docked into the hAChE X-ray structure, co-crystallized with donepezil (PDB ID: 4EY7). The reported experimental pK_a value is 8.82.[27] Marvin estimation is 8.62; therefore, the molecules are mostly protonated. For comparison, both protonated and non-protonated forms were considered. The donepezil position obtained by AutoDock reproduced the X-ray position very well (RMSD = 0.59 Å), and the position obtained by FlexX was slightly shifted, but still reproduced it sufficiently (RMSD = 1.26 Å). A detailed description of this procedure is provided in the Supporting Information (Figures SI-1, SI-2).

The pK_a values of the two nitrogen atoms in alkyl chains estimated for the most active AChE inhibitor **3d** by ChemAxon Marvin were 8.32 and 8.93; by ACD/I-Lab, 8.16 and 8.20. Despite the good agreement between these estimates through two different tools, they are significantly different from experimentally derived values, which were much more acidic (5.28 and 6.49 by pH-metric titration; see details in Supporting Information). Because of the low experimental pK_a values, docking results for the neutral ligand forms were of particular interest.

Binding free energies for AutoDock- and FlexX-docked positions of compound **3d** inside the whole gorge and PAS only with all used targets are presented in the Supporting Information (Figure SI-3). The best binding positions obtained by AutoDock for compound **3d** were with the target from the X-ray structure of hAChE co-crystallized with donepezil (4EY7). Binding with hAChE co-crystallized with Fas-2 (4EY8) and mAChE was considerably weaker and similar to the binding observed with hBChE. This is in agreement with the experimentally determined high selectivity described above. The binding free energy difference between the mono-protonated form with highest binding affinity and the neutral form (Supporting Information, Figure SI-4A,B) is not dramatic: 0.74 kcal mol^{-1}; therefore, neither establish many specific interactions.

Binding free energies calculated by AutoDock for positions obtained by FlexX were considerably lower with a significantly higher dispersion of values between different ligand forms (Supporting Information, Figure SI-3B). The best binding free energies were obtained for positions of the compound inside apo-hAChE after molecular mechanics (MM) optimization. Binding with 4EY8 again was notably weaker, and binding with mAChE and hBChE was even weaker still, but gave similar values for mAChE and hBuChE. The major cause for the significantly lower binding energies on positions obtained by FlexX is the interaction of one nitro group with the active site oxyanion hole and the possibility of the formation of a hydrogen bond with the catalytic Ser203 residue in hAChE (Figure 3). The bis-protonated form shows the highest binding affinity (Figure 3A) due to hydrogen bonds between the second nitro group and PAS residues. Binding of the neutral form was 1.6 kcal mol^{-1} weaker, due to less specific interactions in the PAS (Figure 3B).

For other compounds under consideration, the difference between results obtained by AutoDock and FlexX was retained. Among binding positions generated by AutoDock for five compounds, the best binding affinities were obtained with apo-hAChE as a target after MM optimization (Supporting Information, Figure SI-5A), and for six compounds with hAChE co-crystallized with donepezil (4EY7; Figure SI-5B). Regarding the binding positions obtained by FlexX, the best binding energies of all compounds were with apo-hAChE after MM optimization (Figure SI-5C). There is no docked position obtained by AutoDock with the nitro group inside the active site and oxyanion hole, whereas FlexX results mostly place it there.

Quite reasonably, the binding energies for positions in the PAS depend on the target far less strictly than for positions oc-

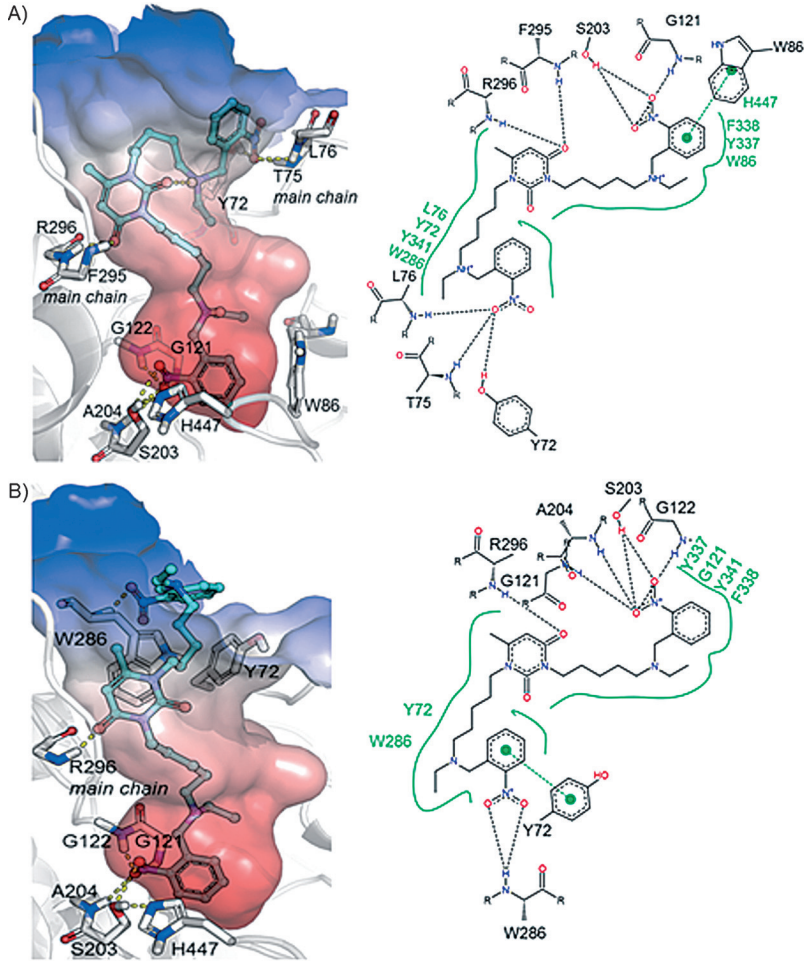

Figure 3. Docked positions of compound **3 d** obtained by FlexX inside the hAChE gorge (PDB ID: 4EY7), showing 3D (left) and 2D (right) images. A) Position with the highest binding affinity of the bis-protonated form of **3 d**; B) position of the neutral form.

cupying active site. Nevertheless, binding with hBChE structures is considerably weaker than with AChE structures. Also, the difference in binding energies between positions obtained by AutoDock and FlexX is less prominent.

A specific feature of binding positions in the PAS by compound **3 d** obtained with AutoDock is that one compound end enters the gorge, blocking it, while the second one binds to the cleft at the edge of the PAS (Figure 4). The difference in binding energies for the bis-protonated and uncharged forms of compounds is 0.6 kcal mol^{-1} (target 4EY7). This indicates that charge is not important for binding. Residues forming a cleft at the PAS edge and that interact with the ligand are Gln279, Asn283, and Tyr72. Positions obtained by FlexX are close to positions obtained by AutoDock (Supporting Information, Figure SI-6). However, taken together, the best positions of all compounds obtained by AutoDock (Supporting Information, Figure SI-7 A) and FlexX (Supporting Information, Figure SI-7 B) show that positions obtained by FlexX are more deeply buried into the gorge, but interact with the PAS edge to a lesser extent.

Molecular docking results indicate that compounds **3 a**–**k** bind to the PAS of AChE with rather high affinity and bind more strongly to the lower parts of the gorge and active site. However, molecular docking results do not reflect the process of ligand trafficking down the gorge through the bottleneck. In particular, experimental pK_a values suggest that these compounds should be de-protonated. It is pointed out that positive charge significantly facilitates substrate and inhibitor trafficking to the active site.[28,29] Thus, calculated binding energies for docked compounds may be used only to compare the different binding positions, but cannot be regarded as actual binding free energies. For calculation of protein–ligand binding free energy with respect to protein conformation, ligand binding to different sites and trafficking through the gorge, molecular dynamics free-energy perturbation (MD FEP) calculations would be helpful. However, the present study focuses specifically on the binding of compounds under consideration with PAS. Thus, computational modeling was limited to docking of compounds inside the full gorge and to PAS of various X-ray AChE conformations with different co-crystallized ligands. This difference was important for binding of compounds in the whole gorge including the active site. Considering the ligand size, the best fit was obtained for the structure with the largest co-crystallized ligand (donepezil), or the structure optimized after saturation with water molecules to compensate the osmotic effect induced by crystallization conditions.[30] Binding to the PAS was not so sensitive to the target conformation, and all results obtained for hAChE and mAChE were very close. Regardless of the possibility of the compounds under consideration to reach the bottom of the gorge, molecular modeling suggests the possibility of tight binding with AChE PAS, blocking the entrance to the gorge. Notably, the cleft at the PAS edge facilitates this binding.

Additionally, this study revealed an important difference in the results obtained by two popular molecular docking programs, FlexX and AutoDock. While the first program revealed positions that were not found by the second program, though performing local search, these positions were considered extremely favorable by it. Lamarckian Genetic Algorithm parameters used in this study were rather high, and docking of one compound took about four days, whereas FlexX docking of the same compound took about 2 h.

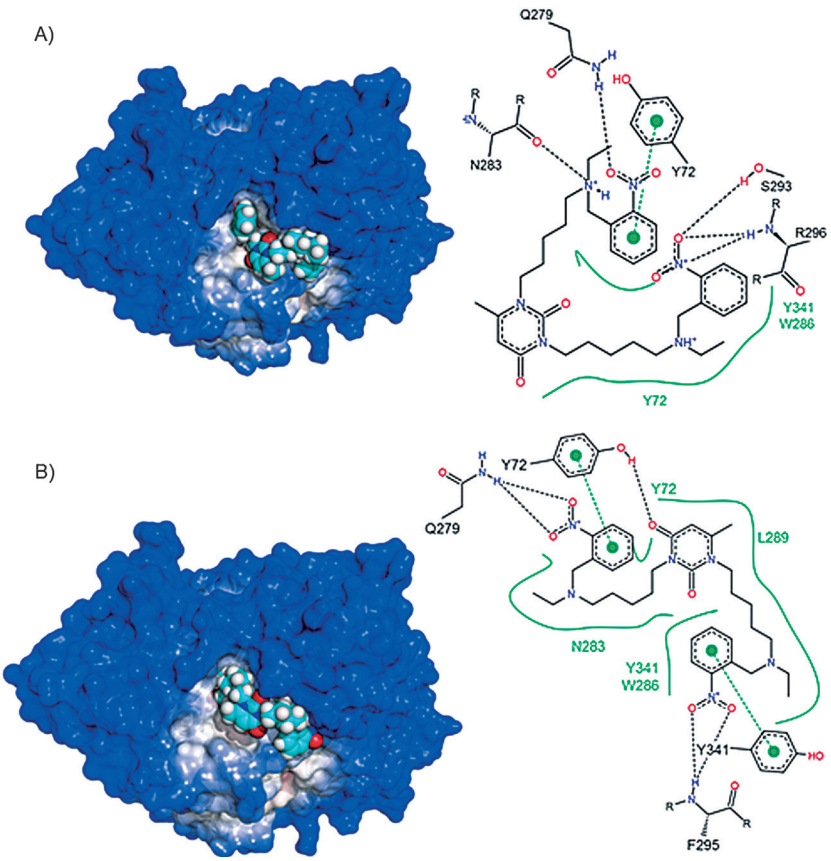

Figure 4. Positions of compound **3d** in its A) charged and B) neutral forms in the PAS of hAChE (PDB ID: 4EY7) obtained with AutoDock. The AChE surface is colored according to distances from the gorge bottom, from red to blue through white.

Another caveat is the use of popular chemoinformatics tools for the estimation of pK_a values. Several comparison studies[31,32] reveal rather good accuracy for of ChemAxon Marvin and ACD/I-Lab. For donepezil, pK_a estimation was very close to the value reported in the literature. In contrast, pK_a estimation for compound **3d**—similar by the two tools—was dramatically far from the experimentally calculated value. Although these tools are very useful, it is necessary to keep in mind that it might be misleading in certain cases.

In vivo biological assays

We evaluated the acute toxicity of the most active compounds discussed in terms of lethal doses (LD_{50}) for mice. We also used LD_{50} values to indicate the ability of the compounds to cross the BBB and to inhibit brain AChE after intraperitoneal (i.p.) injection at the LD_{50} dose. The parameters obtained are summarized in Table 2.

The most potent AChE inhibitors **3d,e,f,j** (Table 1) exhibit the lowest LD_{50} values ($< 100\ mg\,kg^{-1}$). All compounds are able to permeate the BBB. There is no clear relationship between in vitro inhibition of AChE and BChE by the compounds and their in vivo potency to inhibit brain AChE. In particular, in vitro effective AChE inhibitors **3a,f,j** show the weakest inhibitory potency against brain AChE. However, the most effective in vitro AChE inhibitors **3b,d,e,k** inhibit brain AChE by more than 50%.

Compound **3d** is the most effective brain AChE inhibitor. The ability of compound **3d** to block in vitro AChE-induced $A\beta_{1-40}$ aggregation was studied using a thioflavin T (ThT) fluorescent probe. Compound **3d** at 10 nM, exhibited significant ($35 \pm 9\%$) inhibitory activity toward human AChE-induced Aβ aggregation (Figure 5). This compound was studied in vivo for the treatment of memory impairment on an AD model. In particular, the effect of compound **3d** on spatial memory was evaluated in two mouse models of AD (scopolamine and transgenic APP/PS1 models).

Scopolamine i.p. injection ($1\ mg\,kg^{-1}$) induced a significant decrease in correct choice percentage in the T-maze, as well as a decrease in the percentage of mice reaching the criterion for learning the task to day 14. This memory deficit was rescued to some extent either by treatment with compound **3d** ($5\ mg\,kg^{-1}$) or donepezil ($0.75\ mg\,kg^{-1}$) (Figure 6). Interestingly, higher doses of compound **3d** (10 and $15\ mg\,kg^{-1}$) produced less therapeutic effect on spatial memory deficit.

Groups of APP/PS1 mice showed a threefold lower percentage of reaching behavioral criterion and a lower percentage of correct choice in the T-maze alternation task relative to wild-type mice, whereas compound **3d** ($5\ mg\,kg^{-1}$) or donepezil

Table 2. LD_{50} values of AChE inhibitors and percent inhibition of brain AChE after i.p. injection at the LD_{50} dose.

Compd	LD_{50} [$mg\,kg^{-1}$][a]	Inhibition [%][b]
3a	281	38 ± 6
3b	285	59 ± 5
3c	408	51 ± 11
3d	51	71 ± 1
3e	90	49 ± 16
3f	64	6 ± 2
3i	245	46 ± 11
3j	93	3 ± 1
3k	90	58 ± 11

[a] Data represent the mean of five experiments, each carried out with six replicates. [b] Percent inhibition of brain AChE after i.p. injection at the LD_{50} dose; data represent the mean ± SEM ($n = 3$); brain samples of control group ($n = 3$) were used as a control (100% AChE activity).

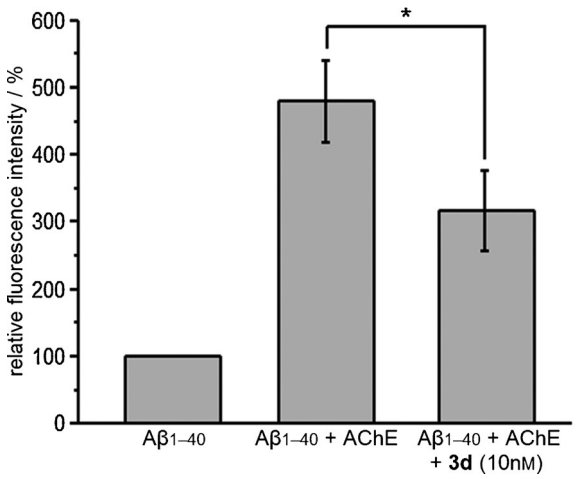

Figure 5. Fluorescence intensity of ThT emission spectra with excitation at λ 446 nm and emission at λ 490 nm in the presence of $A\beta_{1-40}$, $A\beta_{1-40}$ + AChE, and $A\beta_{1-40}$ + AChE + **3 d** (*$p < 0.05$; statistical analysis was performed with the Mann–Whitney test).

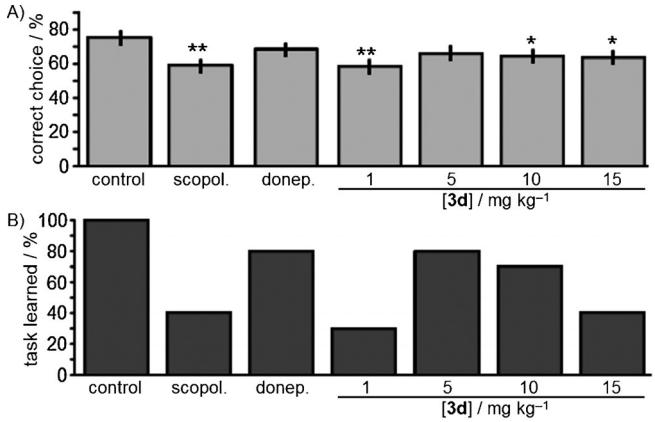

Figure 6. Effect of compound **3 d** on spatial memory performance in an AD scopolamine model in mice. Values represent percentage A) correct choice and B) reaching the criterion of learning the task to day 14 in experimental groups of mice (see Table SI-1, Supporting Information). Mean values ± SEM are shown (*$p < 0.05$, **$p < 0.01$ relative to control group; statistical analysis was performed with the Mann–Whitney test). Control: vehicle alone; [scopolamine] = 1 mg kg^{-1}; [donepezil] = 0.75 mg kg^{-1}.

treatment effectively rescued these parameters in APP/PS1 mice (Figure 7).

Treatment with compound **3 d** (5 mg kg^{-1}) for 14 days significantly decreased the percentage of summary area and number of Aβ peptide deposits visualized in sections of cerebral cortex, dentate gyrus, and hippocampal CA3 area in APP/PS1 mice (Figure 8). The most prominent decrease in Aβ load by compound **3 d** treatment was found in CA3 area and cerebral cortex (Figure 9). Meanwhile, donepezil treatment (1 mg kg^{-1}) for 14 days significantly decreased Aβ load in cerebral cortex, but not in dentate gyrus and CA3 area (Figure 10).

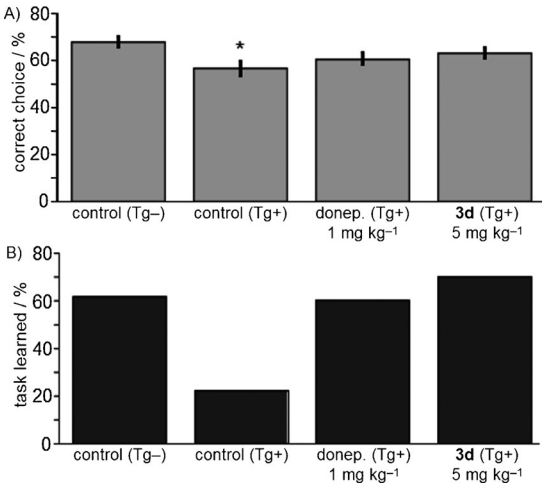

Figure 7. Effect of compound **3 d** on spatial memory performance of APP/PS1 mice (transgenic (Tg) AD model). Values represent percentage A) correct choice and B) reaching the criterion of learning the task to day 14 in experimental groups of mice (see Table SI-1, Supporting Information). Mean values ± SEM are shown (*$p < 0.05$ relative to control group; statistical analysis was performed with the Mann–Whitney test).

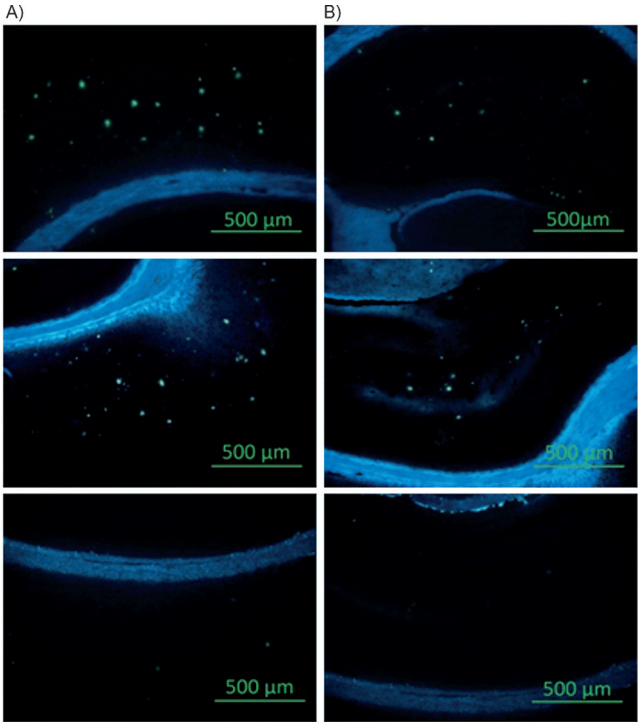

Figure 8. Visualization of Aβ peptide load in brain sections of APP/PS1 mice. A) Hippocampal and B) cortical brain sections of APP/PS1 mice stained with thioflavin S in control (upper panels) or after treatment with donepezil (middle panels) or compound **3 d** (lower panels).

Conclusions

In summary, a series of 1,3-bis[ω-(substituted benzylethylamino)alkyl]-6-methyluracils were designed, synthesized, and evaluated as selective AChE inhibitors. Molecular modeling studies of the compounds indicated that they are able to bind strongly with AChE PAS, regardless of their protonation state. More-

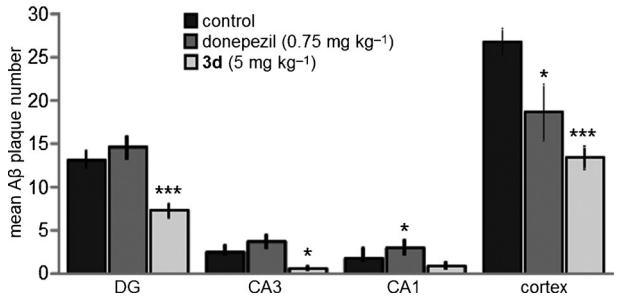

Figure 9. Number of thioflavin S fluorescent spots on images of sections of dentate gyrus (DG), CA3 (CA3) and CA1 (CA1) hippocampal areas, and cerebral cortex (cortex). Mean values ± SEM are shown (*$p < 0.05$, ***$p < 0.001$ relative to control; statistical analysis was performed with the Mann–Whitney test).

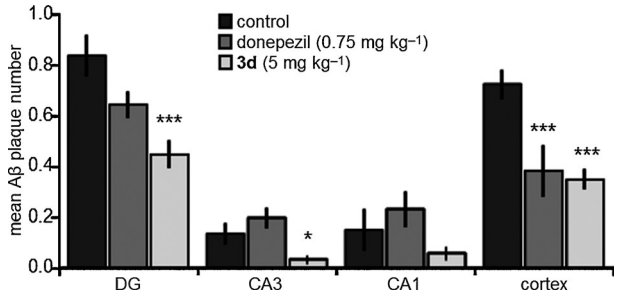

Figure 10. Percentage of total area of thioflavin S fluorescent spots on images of dentate gyrus sections (DG), CA3 (CA3) and CA1 (CA1) hippocampal areas, and cerebral cortex (cortex). Mean values ± SEM are shown (*$p < 0.05$, ***$p < 0.001$ relative to control; statistical analysis was performed with the Mann–Whitney test).

over, the cleft at the PAS edge facilitates this binding. Thus, binding of these 6-methyluracil derivatives blocks the entrance of the gorge, causing inhibition of the esterase activity of AChE. In addition, by masking the PAS area, they impair the role of PAS in chaperoning Aβ aggregation. In vivo experiments showed that the most potent AChE inhibitor **3d** improved working memory in the APP/PS1 transgenic mice and significantly decreased the number and area of Aβ plaques in the brain. Thus, compound **3d** is a promising candidate as a bifunctional inhibitor of AChE for the treatment of AD. Work is in progress to determine the pharmacokinetic parameters of selected compounds. In addition, high-throughput screening of new 6-methyluracil derivatives has been undertaken. The aim is to select drug candidates with long residence time on AChE to improve efficacy, and rapid pharmacokinetics to minimize unwanted side effects.

Experimental Section

Chemistry

General methods: NMR experiments were carried out with Bruker AVANCE-400 spectrometers [400.1 MHz (^{1}H), 100.6 MHz (^{13}C)]. MALDI-TOF mass spectra were recorded on a Bruker ULTRAFLEX mass spectrometer using *p*-nitroaniline as matrix, under the following conditions: Nd:YAG laser, $\lambda = 355$ nm, linear mode without mass spectra accumulation. IR spectra were recorded on a Vector 22 FTIR spectrometer (Bruker) in the 4000–400 cm^{-1} range at a resolution of 1 cm^{-1}. Micro-elemental analysis data were obtained on a CHN-3 analyzer, and were within ± 0.3 % of theoretical values for C, H, and N. Melting points were measured on a Boetius hot-stage apparatus. Thin-layer chromatography was performed on Silufol-254 plates (solvent system: Et_2O or EtOAc/MeOH mixture); visualization of spots was carried out under UV light ($\lambda = 254$ nm). For column chromatography, silica gel 60 mesh (Fluka) was used. All solvents were dried according to standard protocols.

Initial compounds 5 a–c: The syntheses of initial compounds 1,3-bis(4-ethylaminobutyl)-6-methyluracil (**5 a**), 1,3-bis(5-ethylaminopentyl)-6-methyluracil (**5 b**), and 1,3-bis(6-ethylaminohexyl)-6-methyluracil (**5 c**) were reported previously.[24,25]

Synthesis of compounds 3 a–k. General procedure: A mixture of diamine **5 a–c** (5.0 mmol), substituted benzyl bromide **4** (10.0 mmol) and K_2CO_3 (3.45 g, 25.0 mmol) was stirred in CH_3CN (150 mL) at 73–78 °C for 8 h. The precipitate was filtered off. The solution was concentrated to 10–15 mL and transferred to a column with SiO_2. The column was successively washed with petroleum ether (PE), 1:1 PE/Et_2O mixture and Et_2O. The target compounds **3 a–k** were isolated from the Et_2O fractions.

1,3-Bis[4-(*o*-nitrobenzylethylamino)butyl]-6-methyluracil (3 a): Yield 42 %; oil; IR (neat): $\tilde{\nu}_{max} = 2967$, 1701, 1661, 1528, 1449, 1362, 1302, 1208, 1063, 859, 730 cm^{-1}; ^{1}H NMR: $\delta = 7.77$–7.74 (m, 2H, 2ArH), 7.61–7.51 (m, 4H, 4ArH), 7.38–7.34 (m, 2H, 2ArH), 5.54 (s, 1H, $C^5_{uracil}H$), 3.89–3.86 (m, 2H, $N^3_{uracil}CH_2$), 3.83 (s, 2H, CH_2Ph), 3.82 (s, 2H, CH_2Ph), 3.77–3.72 (m, 2H, $N^1_{uracil}CH_2$), 2.51–2.42 (m, 8H, 4NCH_2), 2.27 (s, 3H, $C^6_{uracil}CH_3$), 1.58–1.55 (m, 4H, 2CH_2), 1.46–1.43 (m, 4H, 2CH_2), 0.99–0.94 ppm (m, 6H, 2CH_3); ^{13}C NMR: $\delta = 161.82$, 151.67, 150.76, 149.57, 149.26, 135.72, 134.99, 132.11, 131.85, 130.71, 130.52, 127.38, 126.98, 123.81, 101.30, 59.99, 55.21, 54.83, 52.87, 52.80, 47.47, 47.36, 44.70, 40.75, 26.51, 25.10, 24.24, 24.11, 19.34, 11.35, 11.15 ppm; MALDI-MS (*m/z*): calcd for $C_{31}H_{42}N_6O_6$ $[M-H]^+$, $[M-C_7H_6NO_2]^+$ 593.3, 458.3, respectively, found: 593.3, 458.1; Anal. calcd for $C_{31}H_{42}N_6O_6$: C 62.61, H 7.12, N 14.13, found: C 62.64, H 7.10, N 14.11.

1,3-Bis[4-(*o*-trifluoromethylbenzylethylamino)butyl]-6-methyluracil (3 b): Yield 46 %; oil; IR (neat): $\tilde{\nu}_{max} = 2968$, 1703, 1665, 1528, 1452, 1363, 1313, 1259, 1157, 1120, 1058, 817, 771 cm^{-1}; ^{1}H NMR: $\delta = 7.92$–7.87 (m, 2H, 2ArH), 7.60–7.57 (m, 2H, 2ArH), 7.50–7.47 (m, 2H, 2ArH), 7.31–7.27 (m, 2H, 2ArH), 5.54 (s, 1H, $C^5_{uracil}H$), 3.92–3.89 (m, 2H, $N^3_{uracil}CH_2$), 3.77–3.74 (m, 2H, $N^1_{uracil}CH_2$), 3.70 (s, 2H, CH_2Ph), 3.69 (s, 2H, CH_2Ph), 2.54–2.45 (m, 8H, 4NCH_2), 2.17 (s, 3H, $C^6_{uracil}CH_3$), 1.65–1.61 (m, 4H, 2CH_2), 1.52–1.48 (m, 4H, 2CH_2), 1.04–1.00 ppm (m, 6H, 2CH_3); ^{13}C NMR: $\delta = 162.11$, 151.96, 150.81, 131.68, 131.63, 125.48, 125.32, 101.68, 54.00, 53.99, 53.91, 53.34, 53.19, 47.99, 47.73, 45.02, 41.15, 26.80, 25.49, 24.64, 19.58, 11.88 ppm; MALDI-MS (*m/z*): calcd for $C_{33}H_{42}F_6N_4O_2$ $[M-H]^+$ 639.3, found: 639.1; Anal. calcd for $C_{33}H_{42}F_6N_4O_2$: C 61.86, H 6.61, F 17.79, N 8.74, found: C 61.81, H 6.62, F 17.75, N 8.71.

1,3-Bis[4-(2-nitro-6-fluorobenzylethylamino)butyl]-6-methyluracil (3 c): Yield 46 %; white solid; mp: 98–99 °C; IR (KBr): $\tilde{\nu}_{max} = 2945$, 1688, 1662, 1618, 1538, 1467, 1373, 1249, 1077, 797, 728 cm^{-1}; ^{1}H NMR: $\delta = 7.48$–7.46 (m, 2H, 2ArH), 7.39–7.35 (m, 2H, 2ArH), 7.26–7.23 (m, 2H, 2ArH), 5.56 (s, 1H, $C^5_{uracil}H$), 3.89–3.86 (m, 2H, $N^3_{uracil}CH_2$), 3.85 (s, 2H, CH_2Ph), 3.84 (s, 2H, CH_2Ph), 3.78–3.74 (m, 2H, $N^1_{uracil}CH_2$), 2.45–2.38 (m, 8H, 4NCH_2), 2.27 (s, 3H, $C^6_{uracil}CH_3$), 1.55–1.51 (m, 4H, 2CH_2), 1.43–1.39 (m, 4H, 2CH_2), 0.95–0.91 ppm (m, 6H, 2CH_3); ^{13}C NMR: $\delta = 161.89$, 161.60, 159.61, 151.71, 151.31, 151.26, 151.22, 150.93, 128.41, 128.34, 128.19, 128.12, 122.47,

122.24, 122.11, 119.47, 118.69, 118.57, 118.50, 118.38, 101.30, 52.59, 46.77, 44.69, 40.71, 26.52, 25.08, 23.93, 23.43, 19.36, 10.64 ppm; MALDI-MS (*m/z*): calcd for $C_{31}H_{40}F_2N_6O_6$ $[M-H]^+$, $[M-C_7H_5FNO_2]^+$ 630.3, 476.3, respectively, found: 629.2, 476.0; Anal. calcd for $C_{31}H_{40}F_2N_6O_6$: C 59.04, H 6.39, F 6.02, N 13.33, found: C 59.00, H 6.42, F 6.08, N 13.29.

1,3-Bis[5-(*o*-nitrobenzylethylamino)pentyl]-6-methyluracil (3 d): Yield 74%; oil; IR (neat): $\tilde{\nu}_{max}=2935$, 1700, 1661, 1528, 1449, 1362, 1056, 730 cm^{-1}; ^1H NMR: $\delta=7.77–7.74$ (m, 4H, 4ArH), 7.53–7.50 (m, 2H, 2ArH), 7.38–7.35 (m, 2H, 2ArH), 5.54 (s, 1H, $C^5_{uracil}H$), 3.89–3.86 (m, 2H, $N^3_{uracil}CH_2$), 3.82 (brs, 4H, $2CH_2Ph$), 3.77–3.74 (m, 2H, $N^1_{uracil}CH_2$), 2.45–2.40 (m, 8H, $4NCH_2$), 2.22 (s, 3H, $C^6_{uracil}CH_3$), 1.58–1.55 (m, 4H, $2CH_2$), 1.46–1.43 (m, 4H, $2CH_2$), 1.30–1.24 (m, 4H, $2CH_2$), 0.99–0.94 ppm (m, 6H, $2CH_3$); ^{13}C NMR: $\delta=161.64$, 151.35, 149.43, 149.21, 135.25, 134.89, 131.90, 131.73, 130.61, 130.48, 127.22, 127.01, 123.59, 115.52, 100.89, 95.63, 54.97, 54.72, 52.89, 52.66, 47.15, 47.06, 44.59, 40.58, 28.22, 26.95, 26.20, 26.10, 24.21, 23.89, 19.15, 11.14, 10.91 ppm; MALDI-MS (*m/z*): calcd for $C_{33}H_{46}N_6O_6$ $[M-H]^+$ 621.3, found: 621.2; Anal. calcd for $C_{33}H_{46}N_6O_6$: C 63.65, H 7.45, N 13.49, found: C 63.68, H 7.42, N 13.53.

1,3-Bis[5-(*o*-trifluoromethylbenzylethylamino)pentyl]-6-methyluracil (3 e): Yield 58%; oil; IR (neat): $\tilde{\nu}_{max}=2968$, 1703, 1665, 1453, 1364, 1314, 1259, 1157, 1120, 1058, 1036, 817, 771 cm^{-1}; ^1H NMR: $\delta=7.92–7.87$ (m, 2H, 2ArH), 7.60–7.56 (m, 2H, 2ArH), 7.51–7.47 (m, 2H, 2ArH), 7.30–7.26 (m, 2H, 2ArH), 5.54 (s, 1H, $C^5_{uracil}H$), 3.92–3.88 (m, 2H, $N^3_{uracil}CH_2$), 3.77–3.73 (m, 2H, $N^1_{uracil}CH_2$), 3.70 (brs, 4H, $2CH_2Ph$), 2.52–2.44 (m, 8H, $4NCH_2$), 2.18 (s, 3H, $C^6_{uracil}CH_3$), 1.63–1.60 (m, 4H, $2CH_2$), 1.52–1.48 (m, 4H, $2CH_2$), 1.37–1.34 (m, 4H, $2CH_2$), 1.04–0.98 ppm (m, 6H, $2CH_3$); ^{13}C NMR: $\delta=162.03$, 151.84, 150.80, 139.98, 139.80, 131.54, 131.51, 129.93, 129.91, 126.21, 126.06, 125.83, 125.33, 125.88, 101.49, 53.91, 53.91, 53.84, 53.50, 53.32, 47.74, 47.62, 44.94, 41.11, 28.68, 27.38, 26.88, 26.79, 24.70, 24.43, 19.43, 11.78 ppm; MALDI-MS (*m/z*): calcd for $C_{35}H_{46}F_6N_4O_2$ $[M-H]^+$ 667.3, found: 667.3; Anal. calcd for $C_{35}H_{46}F_6N_4O_2$: C 62.86, H 6.93, F 17.05, N 8.38, found: C 62.89, H 6.94, F 17.00, N 8.43.

1,3-Bis[5-(2-nitro-6-fluorobenzylethylamino)pentyl]-6-methyluracil (3 f): Yield 48%; oil; IR (neat): $\tilde{\nu}_{max}=2937$, 1702, 1663, 1620, 1538, 1468, 1369, 1248, 1182, 1054, 795, 731 cm^{-1}; ^1H NMR: $\delta=$ 7.50–7.47 (m, 2H, 2ArH), 7.36–7.33 (m, 2H, 2ArH), 7.27–7.24 (m, 2H, 2ArH), 5.54 (s, 1H, $C^5_{uracil}H$), 3.88–3.84 (m, 2H, $N^3_{uracil}CH_2$), 3.83 (s, 4H, $2CH_2Ph$), 3.77–3.74 (m, 2H, $N^1_{uracil}CH_2$), 2.43–2.40 (m, 4H, $2NCH_2$), 2.36–2.31 (m, 4H, $2NCH_2$), 2.24 (s, 3H, $C^6_{uracil}CH_3$), 1.57–1.52 (m, 4H, $2CH_2$), 1.39–1.36 (m, 4H, $2CH_2$), 1.24–1.19 (m, 4H, $2CH_2$), 0.93–0.90 ppm (m, 6H, $2CH_3$); ^{13}C NMR: $\delta=161.87$, 161.84, 159.37, 151.67, 151.37, 151.34, 150.98, 128.47, 128.37, 128.24, 122.70, 122.24, 122.53, 119.55, 119.52, 118.72, 118.49, 101.22, 52.56, 46.86, 46.78, 46.29, 44.89, 40.85, 28.43, 27.18, 26.11, 25.80, 24.40, 24.02, 19.44, 10.64, 10.44 ppm; MALDI-MS (*m/z*): calcd for $C_{33}H_{44}F_2N_6O_6$ $[M-H]^+$, $[M-C_7H_5FNO_2]^+$ 657.3, 504.3, respectively, found: 657.3, 504.1; Anal. calcd for $C_{33}H_{44}F_2N_6O_6$: C 60.17, H 6.73, F 5.77, N 12.76, found: C 60.21, H 6.70, F 5.80, N 12.73.

1,3-Bis[5-(2,4-ditrifluoromethylbenzylethylamino)pentyl]-6-methyluracil (3 g): Yield 54%; oil; IR (neat): $\tilde{\nu}_{max}=2969$, 1705, 1666, 1449, 1434, 1347, 1276, 1169, 1129, 1053, 910, 859, 674 cm^{-1}; ^1H NMR: $\delta=8.13–8.09$ (m, 2H, 2ArH), 7.86–7.83 (m, 2H, 2ArH), 7.80–7.77 (m, 2H, 2ArH), 5.55 (s, 1H, $C^5_{uracil}H$), 3.92–3.89 (m, 2H, $N^3_{uracil}CH_2$), 3.79–3.76 (m, 2H, $N^1_{uracil}CH_2$), 3.75 (brs, 4H, $2CH_2Ph$), 2.55–2.46 (m, 8H, $4NCH_2$), 2.21 (s, 3H, $C^6_{uracil}CH_3$), 1.63–1.60 (m, 4H, $2CH_2$), 1.51–1.48 (m, 4H, $2CH_2$), 1.37–1.34 (m, 4H, $2CH_2$), 1.04–1.00 (m, 6H, $2CH_3$); ^{13}C NMR: $\delta=162.03$, 151.84, 150.80, 139.98, 139.80, 131.54, 131.51, 129.91, 128.90, 128.76, 126.21, 126.06, 125.83, 125.33, 125.88, 125.54, 125.48, 101.49, 53.91, 53.91, 53.84, 53.50, 53.32, 47.74, 47.62, 44.94, 41.11, 28.68, 27.38, 26.88, 26.79, 24.70, 24.43, 19.43, 11.78 ppm; MALDI-MS (*m/z*): calcd for $C_{37}H_{44}F_{12}N_4O_2$ $[M-H]^+$ 803.3, found: 803.3; Anal. calcd for $C_{37}H_{44}F_{12}N_4O_2$: C 55.22, H 5.51, F 28.33, N 6.96, found: C 55.26, H 5.52, F 28.28, N 7.00.

1,3-Bis[5-(2-trifluoromethyl-6-fluorobenzylethylamino)pentyl]-6-methyluracil (3 h): Yield 84%; oil; IR (neat): $\tilde{\nu}_{max}=2938$, 1703, 1664, 1460, 1360, 1315, 1248, 1128, 1052, 803, 722 cm^{-1}; ^1H NMR: $\delta=$ 7.46–7.43 (m, 2H, 2ArH), 7.34–7.31 (m, 2H, 2ArH),7.21–7.18 (m, 2H, 2ArH), 5.53 (s, 1H, $C^5_{uracil}H$), 3.89–3.86 (m, 2H, $N^3_{uracil}CH_2$), 3.76–3.73 (m, 2H, $N^1_{uracil}CH_2$), 3.71 (brs, 4H, $2CH_2Ph$), 2.50–2.47 (m, 4H, $2NCH_2$), 2.43–2.40 (m, 4H, $2NCH_2$), 2.20 (s, 3H, $C^6_{uracil}CH_3$), 1.58–1.55 (m, 4H, $2CH_2$), 1.47–1.44 (m, 4H, $2CH_2$), 1.30–1.26 (m, 4H, $2CH_2$), 0.99–0.96 ppm (m, 6H, $2CH_3$); ^{13}C NMR: $\delta=162.03$, 151.84, 150.80, 139.98, 139.80, 131.54, 131.51, 129.93, 129.91, 126.21, 126.06, 125.83, 125.33, 125.88, 119.55, 119.52, 101.49, 53.91, 53.91, 53.84, 53.50, 53.32, 47.74, 47.62, 44.94, 41.11, 28.68, 27.38, 26.88, 26.79, 24.70, 24.43, 19.43, 11.78 ppm; MALDI-MS (*m/z*): calcd for $C_{35}H_{44}F_8N_4O_2$ $[M-H]^+$ 703.3, found: 703.1; Anal. calcd for $C_{35}H_{44}F_8N_4O_2$: C 59.65, H 6.29, F 21.57, N 7.95, found: C 59.69, H 6.27, F 21.63, N 7.90.

1,3-Bis[5-(2,3,4,5,6-pentafluorobenzylethylamino)pentyl]-6-methyluracil (3 i): Yield 60%; oil; IR (neat): $\tilde{\nu}_{max}=2939$, 1704, 1665, 1521, 1503, 1470, 1373, 1301, 1125, 1031, 965, 818, 769 cm^{-1}; ^1H NMR: $\delta=5.56$ (s, 1H, $C^5_{uracil}H$), 3.91–3.88 (m, 2H, $N^3_{uracil}CH_2$), 3.79–3.76 (m, 2H, $N^1_{uracil}CH_2$), 3.70 (brs, 4H, $2CH_2Ph$), 2.50–2.47 (m, 4H, $2NCH_2$), 2.43–2.40 (m, 4H, $2NCH_2$), 2.22 (s, 3H, $C^6_{uracil}CH_3$), 1.64–1.59 (m, 4H, $2CH_2$), 1.54–1.50 (m, 4H, $2CH_2$), 1.36–1.32 (m, 4H, $2CH_2$), 1.06–1.03 ppm (m, 6H, $2CH_3$); ^{13}C NMR: $\delta=151.73$, 150.86, 146.51, 146.48, 146.43, 146.40, 144.62, 144.55, 144.52, 144.43, 139.17, 138.22, 138.12, 138.10, 136.23, 136.11, 136.09, 101.34, 52.47, 52.31, 46.82, 46.79, 44.87, 44.20, 40.90, 28.54, 27.15, 26.46, 26.33, 24.41, 24.21, 19.29, 11.40 ppm; MALDI-MS (*m/z*): calcd for $C_{33}H_{38}F_{10}N_4O_2$ $[M-H]^+$ 711.3, found: 711.1; Anal. calcd for $C_{33}H_{38}F_{10}N_4O_2$: C 55.62, H 5.37, F 26.66, N 7.86, found: C 55.67, H 5.34, F 26.72, N 7.83.

1,3-Bis[5-(*o*-nitrobenzylethylamino)hexyl]-6-methyluracil (3 j): Yield 40%; oil; IR (neat): $\tilde{\nu}_{max}=2934$, 2858, 2807, 1701, 1663, 1529, 1448, 1302, 1060, 731 cm^{-1}; ^1H NMR: $\delta=7.80–7.65$ (m, 4H, 4ArH), 7.55–7.52 (m, 2H, 2ArH), 7.38–7.35 (m, 2H, 2ArH), 5.55 (s, 1H, $C^5_{uracil}H$), 3.90–3.86 (m, 2H, $N^3_{uracil}CH_2$), 3.82 (brs, 4H, $2CH_2Ph$), 3.77–3.74 (m, 2H, $N^1_{uracil}CH_2$), 2.48–2.45 (m, 4H, $2NCH_2$), 2.40–2.37 (m, 4H, $2NCH_2$), 2.24 (s, 3H, $C^6_{uracil}CH_3$), 1.61–1.57 (m, 4H, $2CH_2$), 1.42–1.39 (m, 4H, $2CH_2$), 1.29–1.26 (m, 8H, $4CH_2$), 0.99–0.95 ppm (m, 6H, $2CH_3$); ^{13}C NMR: $\delta=162.00$, 151.78, 150.89, 149.69, 149.51, 135.92, 134.60, 132.20, 132.05, 130.85, 130.74, 127.39, 127.22, 123.93, 123.92, 101.40, 55.27, 55.05, 53.27, 53.04, 47.52, 47.33, 44.93, 41.04, 28.71, 27.39, 26.86, 26.75, 26.70, 26.64, 26.42, 19.48, 11.48, 11.22 ppm; MALDI-MS (*m/z*): calcd for $C_{35}H_{50}N_6O_6$ $[M+H]^+$ 651.4, respectively, found: 651.1; Anal. calcd for $C_{35}H_{50}N_6O_6$: C 64.59, H 7.74, N 12.91, found: C 64.64, H 7.70, N 12.85.

1,3-Bis[6-(*o*-trifluoromethylbenzylethylamino)hexyl]-6-methyluracil (3 k): Yield 56%; oil; IR (neat): $\tilde{\nu}_{max}=2935$, 2860, 2806, 1704, 1665, 1451, 1364, 1313, 1257, 1157, 1120, 1058, 1036, 816, 771 cm^{-1}; ^1H NMR: $\delta=7.91–7.88$ (m, 2H, 2ArH), 7.59–7.56 (m, 2H, 2ArH), 7.51–7.48 (m, 2H, 2ArH), 7.30–7.26 (m, 2H, 2ArH), 5.54 (s, 1H, $C^5_{uracil}H$), 3.90–3.87 (m, 2H, $N^3_{uracil}CH_2$), 3.77–3.74 (m, 2H, $N^1_{uracil}CH_2$), 3.70 (brs, 4H, $2CH_2Ph$), 2.53–2.49 (m, 4H, $2NCH_2$), 2.46–2.42 (m, 4H, $2NCH_2$), 2.20 (s, 3H, $C^6_{uracil}CH_3$), 1.62–1.59 (m, 4H, $2CH_2$), 1.47–1.44 (m, 4H, $2CH_2$), 1.34–1.31 (m, 8H, $4CH_2$), 1.03–0.99 ppm (m, 6H, $2CH_3$); ^{13}C NMR: $\delta=162.05$, 151.88, 150.74, 140.08, 139.95, 131.57, 131.51, 130.00, 129.97, 128.15, 128.08,

127.91, 127.84, 126.20, 126.11, 125.62, 125.60, 125.34, 125.29, 125.24, 125.19, 101.58, 53.93, 53.92, 53.87, 53.85, 53.60, 53.46, 47.77, 47.72, 45.01, 41.17, 28.84, 27.53, 27.08, 27.06, 26.91, 26.81, 26.58, 19.50, 11.87 ppm; MALDI-MS (*m/z*): calcd for $C_{37}H_{50}F_6N_4O_2$ $[M-H]^+$ 695.4, found: 695.2; Anal. calcd for $C_{37}H_{50}F_6N_4O_2$: C 63.78, H 7.23, F 16.36, N 8.04, found: C 63.74, H 7.21, F 16.38, N 8.08.

Potentiometry of compound 3d. pH-Metric titration was performed on an I-160 instrument (Gomel Plant of Measuring Equipment, Belarus) at $25\pm1\,^{\circ}C$ using 8 mM HCl solution in an H_2O/EtOH mixture (80 vol%) with an accuracy of ±0.05 log units. The acidities were determined according to a procedure described elsewhere.[33] The concentration of compound **3d** was 2.04 mM, and the initial volume was 10 mL. The experimental data were processed with pK_a calculation using STALABS software.[34] The procedure of pK_a determination is detailed in the Supporting Information.

Computational methods

Structure preparation: Several X-ray structures of human AChE were reported elsewhere:[35] apo-form (PDB ID: 4EY4, 2.16 Å), co-crystallized with (−)-huperzine A (PDB ID: 4EY5, 2.30 Å), (−)-galantamine (PDB ID: 4EY6, 2.40 Å), donepezil (PDB ID: 4EY7, 2.35 Å) and fasciculin-2 (PDB ID: 4EY8, 2.60 Å). These structures provide basic conformational sampling for molecular docking and were used as targets. For molecular docking, all waters and co-crystallized molecules were removed, and hydrogen atoms were added with respect to the hydrogen bonding network with the Reduce 2.15 tool.[36] Additionally, the structure of apo-hAChE (4EY4) was saturated with water molecules and optimized by molecular mechanics (MM) according to the MM protocol.[30] Mouse AChE (PDB ID: 2HA2,[28] resolution 2.05 Å, X-ray structure and after MM optimization) and human BChE structures (PDB ID: 1P0I,[37] X-ray and prepared according to references [22,38]) were added to the set of targets for molecular docking comparison of data. Because molecular docking cannot invert configuration of tertiary and quaternary nitrogen atoms, for each compound four enantiomers were considered: (*R*,*R*), (*R*,*S*), (*S*,*R*), and (*R*,*R*). Similarly, four protonation states were considered: neutral, bis-protonated, and mono-protonated at each nitrogen atom, making 16 structures for each compound. Additionally, for evaluation purposes donepezil was re-docked into hAChE. Standard Gasteiger charges were assigned. pK_a values for all compounds were estimated with Calculator Plugins of Marvin 6.3.0 (ChemAxon, 2014, www.chemaxon.com) and for **3d** additionally with the ACD/I-Lab PhysChem pK_a module (ilab.acdlabs.com/iLab2/).

Molecular docking: Molecular docking was performed with AutoDock 4.2.6[39] software. The grid box for docking into the full gorge from the mouth and PAS to the active site was $22.5\times22.5\times22.5$ Å^3 for all targets. For docking into PAS, the grid box included part of the gorge located above the bottleneck (Tyr124 and Tyr341) and area above the gorge mouth with dimensions of $30.0\times18.75\times18.75$ Å^3. The main selected Lamarckian Genetic Algorithm[40] parameters were 256 runs, 25×10^6 evaluations, 27×10^4 generations, and population size 300. Another tool used for docking was FlexX[41] (as a part of the LeadIt 2.1.7 software package, BioSolveIt GmbH, 2014, www.biosolveit.de/FlexX/). To compare results obtained by the two programs, docked positions obtained by FlexX additional Local Search runs in AutoDock were performed to derive binding free energy estimations. Images were prepared by PoseView[42] and PyMOL.[43]

Biological studies

In vitro cholinesterase inhibition: Reagents and chemicals: Acetylthiocholine iodide, butyrylthiocholine iodide, recombinant human AChE, BChE from human plasma, and 5,5′-dithiobis-(2-nitrobenzoic) acid (DNTB) were purchased from Sigma–Aldrich. All assays were performed at 25 °C using a PerkinElmer λ25 spectrophotometer at λ 412 nm. Enzyme-catalyzed hydrolysis was carried out in 0.1 M phosphate buffer (pH 8.0) containing 0.25 U AChE or BChE, and 1 mM acetylthiocholine (ATCh) or butyrylthiocholine (BuTCh) as substrates. The tested compounds were pre-incubated with the enzyme for 5 min at 25 °C prior to addition of the substrate and recording hydrolysis kinetics. The rate of substrate hydrolysis as measured by the change in OD_{412} over the course of 2 min was calculated. Sample without inhibitor was used as a control (100% cholinesterase activity). Sample without substrate was used as a blank. IC_{50} (drug concentration required to inhibit enzyme activity by 50%) values were determined with Origin 8.5. Percentage inhibition was calculated by Hill plot.

Studies of AChE inhibition mechanism: For inhibition constant (K_i) determination, various concentrations of compound **3d** were mixed with AChE or BChE in 0.1 M phosphate buffer (pH 8.0). The rate of hydrolysis of acetylthiocholine iodide or butyrylthiocholine iodide was then measured at 25 °C at λ 412 nm using a PerkinElmer λ25 spectrophotometer after the addition of DTNB (0.1 mM final concentration) and substrate. The initial velocity (V_i) of substrate hydrolysis was measured at various substrate (S) concentrations in the range 0.1–0.5 mM. Inhibition constants for AChE were determined from Dixon plot ($1/V_i$ vs. [I]) and Cornish-Bowden transformation ([S]/V_i vs. [I]).[44]

Inhibition of human recombinant AChE-induced Aβ_{1-40} peptide aggregation assay: The thioflavin T (ThT) fluorescence method was used as described.[21] Aβ_{1-40} (Sigma–Aldrich) was lyophilized from 2 mg mL^{-1} 1,1,1,3,3,3-hexafluoro-2-propanol (HFIP) solution. Aβ_{1-40} (2 μL) was incubated in 0.215 M sodium phosphate buffer (pH 8.0) alone or with 16 μL human recombinant AChE (Sigma–Aldrich) in the presence of compound **3d** (2 μL) to give final concentrations of 230 μM Aβ_{1-40}, 2.3 μM AChE, and 10 nM compound **3d**. Following co-incubation at room temperature for 24 h, 180 μL of 1.5 μM ThT in 50 mM glycine/NaOH (pH 8.5) was added. The fluorescence was monitored at λ_{ex} 446 nm. The emission was monitored at λ_{em} 490 nm using a Cary Eclipse fluorescence spectrophotometer (Agilent Technologies, USA). The percent inhibition of AChE-induced aggregation was calculated by the following expression: $100-(IF_i/IF_0\times100)$, in which IF_i and IF_0 are the fluorescence intensities in the presence and absence of the test compound, respectively, minus the fluorescence intensities of the respective blanks. Each assay was conducted in triplicate, and each experiment was repeated at least three independent times.

Acute toxicity evaluation and in vivo BBB permeation assay: Experiments involving animals were performed in accordance with the guidelines set forth by the European Communities Council Directive of November 24, 1986 (86/609/EEC), and the protocol of experiments was approved by the Animal Care and Use Committee of Kazan State Medical University. Toxicological experiments were performed using i.p. injection of the various compounds in mice weighing 20–25 g. Mice were maintained on a 12 h light/dark cycle (light from 7:00 to 19:00) at 20–22 °C and 60–70% relative humidity. Five different doses (determined during preliminary tests) were used with six animals per dose. Animals were observed for 72 h after injection, and symptoms of intoxication were recorded. LD_{50} (dose (mg kg^{-1}) causing lethal effects in 50% of animals) was taken

as a criterion of toxicity. LD_{50} values were determined by the method of Weiss.[45] For in vivo BBB permeation assays, the whole brains were removed 30 min after i.p. injection of an LD_{50} dose of test compound (experimental group, three mice) or after i.p. water injection (control group, three mice). Brains were frozen in liquid nitrogen. Whole-brain homogenates were prepared in a Potter homogenizer with 0.05 M Tris·HCl, 1% Triton X-100, 1 M NaCl, 2 mM EDTA (pH 7.0), at a ratio of 1:2 at 4 °C. The homogenate was centrifuged (10000 rev min^{-1}, $T=4$ °C) for 10 min using an Eppendorf 5430R centrifuge with FA-45-30-11 rotor (Eppendorf AG, Hamburg, Germany). Supernatant (50 μL) was incubated with 5 μL iso-OMPA (final concentration 10^{-4} M) for 30 min. After that the enzyme-catalyzed hydrolysis was started by adding 10 μL of acetylthiocholine (0.01 M) as substrate. After 10, 20, or 30 min incubation with substrate at 25 °C, the reaction was stopped by adding neostigmine (0.1 mM). Samples were diluted in 50 mM phosphate buffer (pH 8.0), and DTNB (0.1 mM) was added. Production of the yellow 5-thio-2-nitrobenzoate anion, resulting from reduction of DTNB by thiocholine (the product of enzymatic hydrolysis of acetylthiocholine), was measured spectrophotometrically. The rate of thiocholine production for 20 min (10^{th}–30^{th} minute) was calculated. Brain samples of the control group were used as control (100% cholinesterase activity). Samples without substrate were used as a blank. All measurements for each brain sample were performed in triplicate.

Memory performance study: Two mouse models of AD were used to evaluate the influence of compound **3d** on spatial memory performance:

Scopolamine model: Administration of scopolamine, a muscarinic receptor antagonist, produces transient receptor blockade, cognitive deficits, and deficits in cerebral metabolism, which can be considered a model for AD.[46] An aqueous solution of scopolamine was injected intraperitoneally to mice 20 min before starting the memory test for 14 days. Mice were assigned to seven groups, including four groups receiving i.p. injection of compound **3d** dissolved in 0.1% water-based ethanol solution at various dosages, donepezil-treated mice (donepezil is conventionally used to treat Alzheimer's disease), positive and negative control groups (Supporting Information, Table SI-1).

Transgenic model: B6C3-Tg(APP695)85Dbo Tg(PSEN1)85Dbo double transgenic (APP/PS1) mice expressing a chimeric mouse/human amyloid precursor protein and a mutant of human presenilin-1. Both mutations are associated with early-onset AD.[47,48] APP/PS1 rodents develop Aβ deposits in the brain and memory impairment by 6–8 months of age.[49] The APP/PS1 mouse line was purchased from Jackson Laboratories (USA) and bred at the Puschino animal facility (Moscow region, Russia) branch of the Shemyakin and Ovchinnikov Institute of Bioorganic Chemistry (Moscow, Russia). APP/PS1 mice at the age of 5–6 months were delivered to Kazan State Medical University (Kazan, Russia), where rodents were housed under standard laboratory conditions. Mice were assigned to four groups, including transgenic animals i.p. injected with compound **3d** or donepezil solution, positive (transgenes injected with water) and negative (wild-type (WT) mice (non-transgenic littermates) injected with water) controls (Supporting Information, Table SI-1).

Behavioral tests: To evaluate spatial memory performance, mice were trained on a reward alternation task[50,51] using a conventional T-maze (OpenScience, Moscow, Russia). Before T-maze testing began, mice were placed on a food-deprivation schedule for three days and then given four days to habituate to the maze. On each of 14 training days, mice were given six pairs of training trials. The first trial of each pair (forced trial) involved one of the goal arm doors being closed, and the mouse was constrained to selecting the opposite arm. The mouse was returned to the start box 15–20 s after consuming the reward (diluted sweetened condensed milk). On the second (free-choice) trial, both goal arm doors were opened, but only the arm opposite the one selected in the forced trial was baited. The criterion for a mouse having learned the rewarded alternation task was three consecutive days of at least five correct responses out of the six free trials.

β-Amyloid peptide load study: For the Aβ peptide load study, mice under anesthesia were transcardially perfused, first with cold phosphate-buffered saline (0.1 M PBS, pH 7.4), then with cold 4% paraformaldehyde (Panreac, Spain) in PBS. The whole brain was removed after decapitation and fixed with 4% paraformaldehyde for 24 h. Frozen frontal sections (20 μm) of mouse brains were sliced on motorized cryostat Microm HM525 (Thermo Scientific, USA). Afterward, sections were stained with Mayer's hematoxylin protocol and 1% ThT solution in water/ethanol (1:1). ThT is a fluorochrome that binds to amyloid fibrils but not to monomers. Thus ThT can be used for measurement of cerebral amyloid load.[52] Thioflavin S stained sections were imaged with UV filter on an Olympus BX51WI fluorescent microscope (Japan). Aβ load was evaluated quantitatively as a number and summary area of thioflavin S fluorescent spots in cerebral cortex and hippocampal images using Image J software.

Acknowledgements

*This work was supported by Russian Science Foundation (RSF) grant 14-50-00014 for the synthesis of inhibitors, their in vitro investigation, molecular modeling, acute toxicity, and in vivo brain AChE inhibition. The study of compound **3d** on scopolamine and transgenic Alzheimer's disease models was supported by Russian Foundation for Basic Research (RFBR) grant 13-00-40286-K. S.V.L. is grateful to the Dynasty Foundation (Russia) for a fellowship. The authors are grateful to the Kazan Department of the Joint Supercomputer Center of the Russian Academy of Sciences, Branch of Federal State Institution "Scientific Research Institute for System Analysis" of the Russian Academy of Sciences for computation time.*

Keywords: 6-methyluracil · acetylcholinesterase · Alzheimer's disease · molecular modeling · reversible inhibitors

[1] P. Davies, A. J. Maloney, *Lancet* **1976**, *308*, 1403.
[2] P. C. Trippier, K. J. Labby, D. D. Hawker, J. J. Mataka, R. B. Silverman, *J. Med. Chem.* **2013**, *56*, 3121–3147.
[3] A. Agis-Torres, M. Sölhuber, M. Fernandez, J. M. Sanchez-Montero, *Curr Neuropharmacol.* **2014**, *12*, 2–36.
[4] J. L. Cummings, *N. Engl. J. Med.* **2004**, *351*, 56–67.
[5] K. G. Mawuenyega, W. Sigurdson, V. Ovod, L. Munsell, T. Kasten, J. C. Morris, K. E. Yarasheski, R. J. Bateman, *Science* **2010**, *330*, 1774.
[6] M. Citron, *Nat. Rev. Drug Discovery* **2010**, *9*, 387–398.
[7] F. Panza, V. Solfrizzi, V. Frisardi, B. P. Imbimbo, C. Capurso, A. D'Introno, A. M. Colacicco, D. Seripa, G. Vendemiale, A. Capurso, A. Pilotto, *Aging. Clin. Exp. Res.* **2009**, *21*, 386–406.
[8] N. C. Inestrosa, M. C. Dinamarca, A. Alvarez, *FEBS J.* **2008**, *275*, 625–632.
[9] G. V. De Ferrari, M. A. Canales, I. Shin, L. M. Weiner, I. Silman, N. C. Inestrosa, *Biochemistry* **2001**, *40*, 10447–10457.
[10] A. Nordberg, C. Ballard, R. Bullock, T. Darreh-Shori, M. Somogyi, *Prim. Care Companion CNS Disord.* **2013**, *15*, DOI: 10.4088/PCC.12r01412, PMC ID: 3733526.

[11] N. C. Inestrosa, A. Alvarez, C. A. Pérez, R. D. Moreno, M. Vicente, C. Linker, O. I. Casanueva, C. Soto, J. Garrido, *Neuron* **1996**, *16*, 881 – 891.
[12] S. Diamant, E. Podoly, A. Friedler, H. Ligumsky, O. Livnah, H. Soreq, *Proc. Natl. Acad. Sci. USA* **2006**, *103*, 8628 – 8633.
[13] E. Podoly, T. Bruck, S. Diamant, N. Melamed-Book, A. Weiss, Y. Huang, O. Livnah, S. Langermann, H. Wilgus, H. Soreq, *Neurodegener Dis.* **2008**, *5*, 232 – 236.
[14] E. C. Hulme, N. J. Birdsall, N. J. Buckley, *Annu. Rev. Pharmacol. Toxicol.* **1990**, *30*, 633 – 673.
[15] N. Mimica, P. Presecki, *Psychiatr. Danubina* **2009**, *21*, 108 – 113.
[16] B. Benyamin, R. P. Middelberg, P. A. Lind, A. M. Valle, S. Gordon, D. R. Nyholt, S. E. Medland, A. K. Henders, A. C. Heath, P. A. Madden, P. M. Visscher, D. T. O'Connor, G. W. Montgomery, N. G. Martin, J. B. Whitfield, *Hum. Mol. Genet.* **2011**, *20*, 4504 – 4514.
[17] L. Pisani, M. Catto, I. Giangreco, F. Leonetti, O. Nicolotti, A. Stefanachi, S. Cellamare, A. Carotti, *ChemMedChem* **2010**, *5*, 1616 – 1630.
[18] M. Tonelli, M. Catto, B. Tasso, F. Novelli, C. Canu, G. Iusco, L. Pisani, A. De Stradis, N. Denora, A. Sparatore, V. Boido, A. Carotti, F. Sparatore, *ChemMedChem* **2015**, *10*, 1040 – 1053.
[19] I. Bolea, J. Juárez-Jiménez, C. de Los Ríos, M. Chioua, R. Pouplana, F. J. Luque, M. Unzeta, J. Marco-Contelles, A. Samadi, *J. Med. Chem.* **2011**, *54*, 8251 – 8270.
[20] E. García-Palomero, P. Munoz, P. Usan, P. Garcia, E. Delgado, C. De Austria, R. Valenzuela, L. Rubio, M. Medina, A. Martínez, *Neurodegener. Dis.* **2008**, *5*, 153 – 156.
[21] E. Viayna, I. Sola, M. Bartolini, A. De Simone, C. Tapia-Rojas, F. G. Serrano, R. Sabaté, J. Juárez-Jiménez, B. Pérez, F. J. Luque, V. Andrisano, M. V. Clos, N. C. Inestrosa, D. Muñoz-Torrero, *J. Med Chem.* **2014**, *57*, 2549 – 2567.
[22] K. A. Anikienko, E. A. Bychikhin, V. S. Reznik, V. D. Akamsin, I. V. Galyametdinova, *Chem.-Biol. Interact.* **2008**, *175*, 286 – 292.
[23] V. E. Semenov, R. K. Giniyatullin, S. V. Lushchekina, E. D. Kots, K. A. Petrov, A. D. Nikitashina, O. A. Minnekhanova, V. V. Zobov, E. E. Nikolsky, P. Masson, V. S. Reznik, *MedChemComm* **2014**, *5*, 1729 – 1735.
[24] V. E. Semenov, A. D. Voloshina, E. M. Toroptzova, N. V. Kulik, V. V. Zobov, R. K. Giniyatullin, A. S. Mikhailov, A. E. Nikolaev, V. D. Akamsin, V. S. Reznik, *Eur. J. Med. Chem.* **2006**, *41*, 1093 – 1101.
[25] V. E. Semenov, R. K. Giniyatullin, A. S. Mikhailov, A. E. Nikolaev, S. V. Kharlamov, S. K. Latypov, V. S. Reznik, *Eur. J. Org. Chem.* **2011**, 5423 – 5426.
[26] G. L. Ellman, K. D. Courtney, V. Andres, R. M. Feather-Stone, *Biochem. Pharmacol.* **1961**, *7*, 88 – 95.
[27] S. D. Angelantonio, G. Bernardi, N. B. Mercuri, *Br. J. Pharmacol.* **2004**, *141*, 644 – 652.
[28] Y. Bourne, Z. Radic, G. Sulzenbacher, E. Kim, P. Taylor, P. Marchot, *J. Biol. Chem.* **2006**, *281*, 29256 – 29267.
[29] J. P. Colletier, D. Fournier, H. M. Greenblatt, J. Stojan, J. L. Sussman, G. Zaccai, I. Silman, M. Weik, *EMBO J.* **2006**, *25*, 2746 – 2756.
[30] P. Masson, S. Lushchekina, L. M. Schopfer, O. Lockridge, *Biochem. J.* **2013**, *454*, 387 – 399.
[31] A. C. Lee, G. M. Crippen, *J. Chem. Inf. Model.* **2009**, *49*, 2013 – 2033.
[32] C. Liao, M. C. Nicklaus, *J. Chem. Inf. Model.* **2009**, *49*, 2801 – 2812.
[33] O. Popovych, *Anal. Chem.* **1964**, *36*, 878 – 883.
[34] A. A. Krutikov, V. G. Shtyrlin, A. O. Spiridonov, N. Y. Serov, A. N. Il'yin, E. M. Gilyazetdinov, M. S. Bukharov, *J. Phys. Conf. Ser.* **2012**, *394*, 012031.
[35] J. Cheung, M. J. Rudolph, F. Burshteyn, M. S. Cassidy, E. N. Gary, J. Love, M. C. Franklin, J. J. Height, *J. Med. Chem.* **2012**, *55*, 10282 – 10286.
[36] J. M. Word, S. C. Lovell, J. S. Richardson, D. C. Richardson, *J. Mol. Biol.* **1999**, *285*, 1735 – 1747.
[37] Y. Nicolet, O. Lockridge, P. Masson, J. C. Fontecilla-Camps, F. Nachon, *J. Biol. Chem.* **2003**, *278*, 41141 – 41147.
[38] S. V. Lushchekina, V. S. Polomskikh, S. D. Varfolomeev, P. Masson, *Russ. Chem. Bull.* **2013**, *62*, 2527 – 2537.
[39] G. M. Morris, R. Huey, W. Lindstrom, M. F. Sanner, R. K. Belew, D. S. Goodsell, A. J. Olson, *J. Comput. Chem.* **2009**, *30*, 2785 – 2791.
[40] G. M. Morris, D. S. Goodsell, R. S. Halliday, R. Huey, W. E. Hart, R. K. Belew, A. J. Olson, *J. Comput. Chem.* **1998**, *19*, 1639 – 1662.
[41] B. Kramer, M. Rarey, T. Lengauer, *Proteins Struct. Funct. Bioinf.* **1999**, *37*, 228 – 241.
[42] K. Stierand, M. Rarey, *J. Cheminf.* **2011**, *3*, 21.
[43] The PyMOL Molecular Graphics System, Version 1.7.4, **2014**, Schrödinger LLC.
[44] A. Cornish-Bowden, *Biochem. J.* **1974**, *137*, 143 – 144.
[45] E. S. Weiss, *Am. J. Public Health Nation's Health* **1948**, *38*, 22 – 24.
[46] G. Smith, *Brain Res. Rev.* **1988**, *13*, 103 – 118.
[47] H. W. Querfurth, F. M. La Ferla, *N. Engl. J. Med.* **2010**, *362*, 329 – 344.
[48] M. A. Mukhamedyarov, A. L. Zefirov, *Usp. Fiziol. Nauk* **2013**, *44*, 55 – 71.
[49] A. Savonenko, G. M. Xu, T. Melnikova, J. L. Morton, V. Gonzales, M. P. Wong, D. L. Price, F. Tang, A. L. Markowska, D. R. Borchelt, *Neurobiol. Dis.* **2005**, *18*, 602 – 617.
[50] K. A. Corcoran, Y. Lu, R. S. Turner, S. Maren, *Learn. Mem.* **2002**, *9*, 243 – 252.
[51] R. M. J. Deacon, J. N. P. Rawlins, *Nat. Protoc.* **2006**, *1*, 7 – 12.
[52] M. T. Elghetany, A. Saleem, *Stain Technol.* **1988**, *63*, 201 – 212.

Received: July 27, 2015
Published online on September 28, 2015